Utah State University

DigitalCommons@USU

8-2018

A Non-Equilibrium Molecular Dynamics Study of the Effects of Helium Bubbles on the Thermal Conductivity of ZrC

Tate Shorthill
Utah State University

Recommended Citation

UtahState University
MERRILL-CAZIER LIBRARY

A NON-EQUILIBRIUM MOLECULAR DYNAMICS STUDY OF THE EFFECTS OF

HELIUM BUBBLES ON THE THERMAL CONDUCTIVITY OF ZRC

by

Tate Shorthill

A report submitted in partial fulfillment
of the requirements for the degree

of

MASTER OF SCIENCE

in

Mechanical Engineering

Approved:

Nicholas Roberts, Ph.D.	Ling Liu, Ph.D.
Major Professor	Committee Member

Tadd Truscott, Ph.D.
Committee Member

UTAH STATE UNIVERSITY
Logan, Utah

2018

ABSTRACT

A non-equilibrium molecular dynamics study of the effects of helium bubbles on the

thermal conductivity of ZrC

by

Tate Shorthill, Master of Science

Utah State University, 2018

Major Professor: Dr. Nicholas Roberts
Department: Mechanical & Aerospace Engineering

Zirconium carbide (ZrC) has been proposed as a potential improvement to nuclear

fuel cladding. As such, it is important to characterize its physical properties, particularly

those relating to thermal energy transport. Reactor conditions are known to damage fuel

microstructure over time. While research has been conducted on undamaged and

damaged ZrC, some areas of interest remain. Fission products, such as helium, can

accumulate in pores within the fuel microstructure. Such a case has yet to be

characterized in ZrC fuel cladding.

A non-equilibrium molecular dynamics model was developed to characterize the

thermal properties of ZrC. Fourier's Law allows the thermal conductivity of ZrC to be

determined based on the relationship between heat flux and temperature gradient. The

thermal conductivity of an undamaged ZrC lattice is compared to the thermal

conductivity of a damaged lattice. The values of thermal conductivity demonstrating the

impact of damage from pores and helium-filled pores are reported.

(34 pages)

PUBLIC ABSTRACT

A non-equilibrium molecular dynamics study of the effects of helium bubbles on the

thermal conductivity of ZrC

Tate Shorthill

Zirconium carbide (ZrC) has been proposed as a potential improvement to nuclear fuel containment. As such, it is important to characterize the properties of ZrC. Reactor conditions are known to damage fuel containers over time. While research has been conducted on undamaged and damaged ZrC, some areas of interest remain. Nuclear reaction products, such as helium, can accumulate in bubbles within the fuel microstructure. Such a case has yet to be analyzed in ZrC.

This project relies on computer simulations to model the thermal properties of ZrC. The computer simulation shows how the thermal conductivity of ZrC changes with damage. Two studies, one of damage due to empty bubbles and another of damage due to bubbles filled with helium, are compared to the baseline undamaged ZrC case. The results show a decrease in thermal conductivity with increased damage to the ZrC model.

ACKNOWLEDGMENTS

CONTENTS

LIST OF FIGURES

LIST OF TABLES

INTRODUCTION

The study of materials applicable to the nuclear industry is important. Gen IV nuclear power plants are anticipated to have outlet temperatures from the core of 1000 °C [1]. Elevated temperatures demand the use of safer fuels and improved material properties, particularly those relating to the transport of thermal energy, such as thermal conductivity. Tri-structural isotropic (TRISO) fuel has been the proposed means for improved fuel performance and safety. The TRISO fuel particle is composed of the fissile fuel (UO_2), pyrolytic carbon (PyC), and silicon carbide (SiC). The outer structure of the fuel particle is specifically designed to trap fission gases and contain the fission products (see Figure 1 for example TRISO fuel) [2] [3].
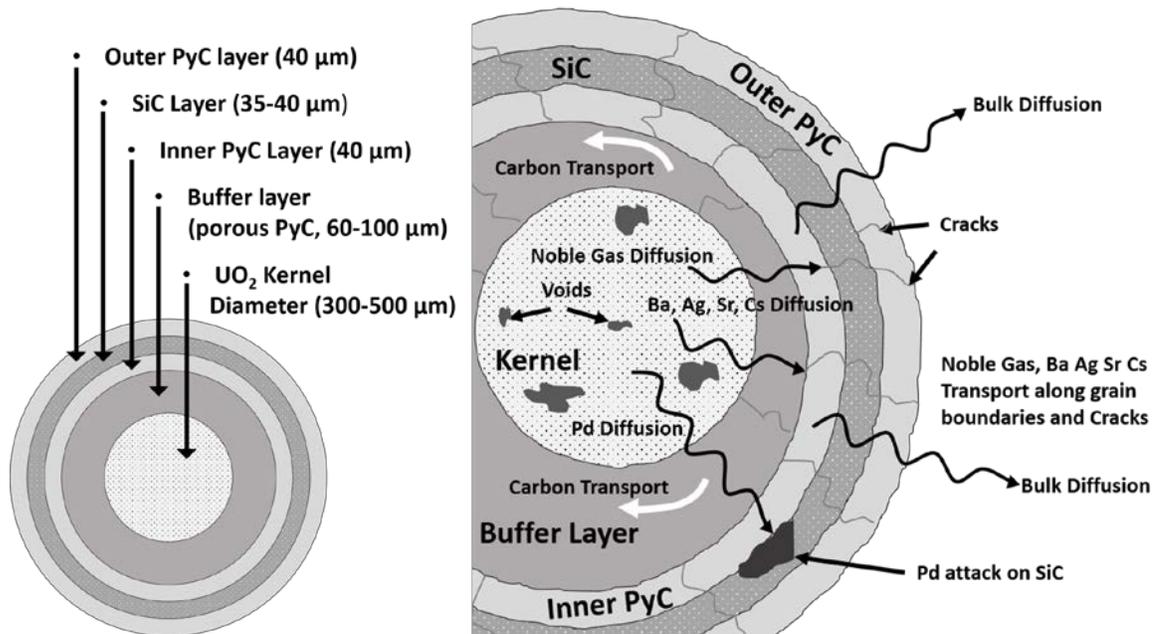
Figure 1: Basic TRISO fuel with layer dimensions (left). The processes found in high burn-up of fuel (right). The image on the right has been reproduced from an image originally from Besmann [4] and found in [3].

It has been noted that TRISO fuels fail or crack due to overpressure and attack from fission products [3]. Of particular concern is CO that is formed when free oxygen generated from fission bonds to the carbon found in the layers of the TRISO fuel, the accumulation of which leads to overpressure and fracture of the TRISO particles. ZrC is known to reduce failures due to CO formation. Porter et al. suggest incorporating a ZrC layer within the TRISO fuel particle to take advantage of the oxygen gettering ability of the ZrC [5], thus providing a potential solution to over pressurization from CO. Figure 2 shows the suggested TRISO fuel with ZrC layer.
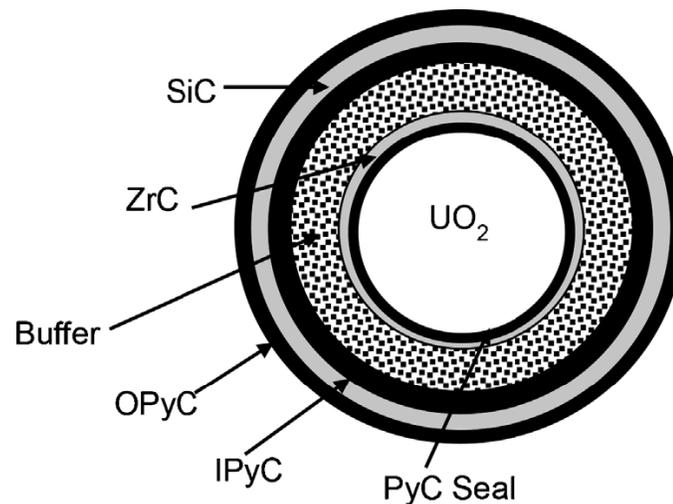
Figure 2: Cross-section of an advanced TRISO fuel particle. Image from Porter et al [5].

A ZrC layer in the TRISO fuel is produced by chemical vapor deposition, a process that can lead to variation in density and stoichiometry [5]. Consequently, thermal conductivity also varies. A review of the literature has shown the thermal conductivity of ZrC between 19-31 W/mK at approximately 300K [6]. Radiation exposure also affects thermal conductivity. Jensen et al. report as much as a 55% reduction in thermal conductivity due to radiation exposure (1.75 dpa at 600 °C by 2.6 MeV proton beam) [7].

Pores formed within the fuel during fission are reported on the order of 10-1000 Å. Fission products such as He, Kr and Xe collect in these bubbles [8]. A molecular dynamics study has shown the effects of pores (empty and filled with He) on the thermal conductivity of UO_2 [7]. It is assumed that the ZrC layer will also experience similar damage and accumulation of fission gasses. It is proposed to investigate ZrC in a similar manner, comparing the effects of pores on the thermal conductivity of the material.

OBJECTIVES

The objectives of this project require the use of Non-Equilibrium Molecular Dynamics (NEMD) to model the thermal properties of ZrC. The simulation applies a steady heat flux to a stable crystal lattice of known dimensions. Fourier's Law is then used to determine the thermal conductivity. This project presents the following:

- A baseline simulation of the thermal conductivity of ZrC performed at 300 K.

- A simulation of the effects of porosity on the thermal conductivity of ZrC performed at 300 K.

- A simulation of the effects of fission gas (helium) within the pores of the sample performed at 300 K.

- A repeat of the three simulations above performed at 1273 K.

METHOD

<u>Molecular Dynamics</u>

Molecular Dynamics (MD) is the study of the behavior of atoms and molecules in motion and their interactions with their surroundings. MD relies on the statistical thermodynamic relations that are used to predict the behaviors and interactions of atoms. Essential to these models is the interatomic potential, which supplies the necessary information to atomic interactions.

The Large-scale Atomic/Molecular Massively Parallel Simulator (LAMMPS) is an advanced MD program developed in part by Sandia National labs and funded primarily by the Department of Energy [9]. As a free-to-use and well-supported program, LAMMPS was the logical choice for performing this research. It can also be used on personal computers, but with larger simulations there is a significant cost in computational time. The initial work of testing the ZrC potential file was done with a personal computer. All subsequent simulations, however, were conducted using the resources of the Center for High Performance Computing at the University of Utah.

<u>Interatomic Potential</u>

The most challenging portion of MD simulations is developing or finding an appropriate interatomic potential for the interactions between atoms and molecules. This study is not focused on the development of new or improved potentials; consequently, the use of existing interatomic potentials was determined appropriate. Online libraries, such NIST interatomic potential repository, are ideal first choice candidates for locating potentials [10]. The ZrC potential used here, however, is not found in one of the more well-known locations.

Duff et al. developed a code that uses information provided by density functional theory (DFT) to generate embedded atom method (EAM) and reference-free modified embedded atom method (MEAM) interatomic potentials. Their example code provides a ZrC potential developed for modeling thermal excitations based on DFT calculations of thermal vibrations near the melting point of ZRC [11]. While the potential is based on vibrations near the melting point of ZrC, it was assumed to be an appropriate starting point in the development of this project. The chief purpose of the baseline simulation, discussed later, is to verify the appropriateness of this chosen ZrC potential.

The introduction of helium in later simulations required that an additional interatomic potential be selected for the He-He, He-Zr and He-C interactions. The Lennard-Jones potential was chosen to model these interactions. He-Zr and He-C potentials were calculated using the Lorenz-Berthelot mixing rules shown below [12] [13].

$$\varepsilon_{ij} = \sqrt{\varepsilon_i \varepsilon_j} \qquad (1)$$

$$\sigma_{ij} = \frac{\sigma_i + \sigma_j}{2} \qquad (2)$$

The mixing rules require the Lennard-Jones parameters for the unmixed atomic interactions (He-He, C-C, and Zr-Zr). The values for these parameters are shown in Table 1. The tabulated results of the Lennard Jones parameters as determined from the mixing rules are shown in Table 2.

<div align="center">Table 1: Lennard Jones Potentials</div>

Potential	ε(eV)	σ(Å)
He-He	0.00219	2.559
C-C	0.002413	3.40
Zr-Zr	0.7382	2.9318

Sourced: [8] [13] [14]

<div align="center">Table 2: Lennard Jones Potentials from Mixing Rules</div>

Potential	ε(eV)	σ(Å)
He-He	0.00219	2.559
He-C	0.002299	2.9795
He-Zr	0.04021	2.7454

Model Development

A 3D crystal lattice for ZrC was placed in the model. The crystal structure for ZrC is rock-salt or, specifically, two interlacing FCC structures (see Figure 3). The base model used in each of the simulations consisted of a single perfect crystal of ZrC. The model shown in Figure 3 is measured in terms of the lattice constants (LC) equivalent to 4.698 Å [15]. It is 14 by 14 by 150 LC in the x, y, and z directions respectively. The model is broken into zones that vary in thickness in the z-direction. The middle test zone of 110 LC is sandwiched between a hot zone and cold zone, each 10 LC. These supply the heat flux to the system. To account for LAMMPS specific requirements, a top and bottom wall of stationary atoms were created to ensure that heat flows in one direction through the test section. Periodic boundaries were selected for all sides of the test zone. These periodic boundaries allow for bulk property measurements of the 110 LC test section, essentially simulating a 0.05 µm thick sample of infinite width.
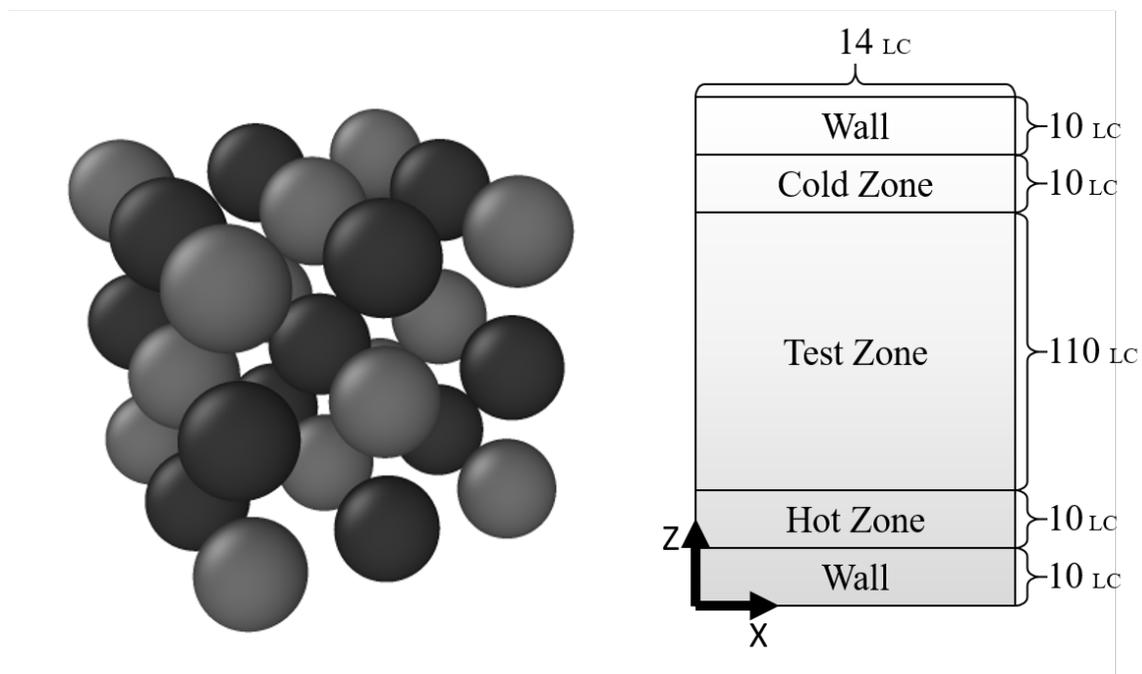
Figure 3: Crystal lattice (left) and model diagram (right). The model diagram shows cross section of rectangular prism 14 x 14 x 150 lattice constants. (LC = 4.698Å)

The simulation relies on the interatomic potentials to define the interactions that take place when the model runs its initial equilibration routines (specifically, the fix NPT, fix NVT, and fix NVE LAMMPS commands).

The fix NPT command performs time integration on non-Hamiltonian (Nose-Hoover style) equations of motion. These equations generate positions and velocities for the isothermal-isobaric ensemble. The process updates the position and velocity for the atoms in each time step. The NVT command performs time integration on the same Nose-Hoover style equations of motion but is performed on the canonical (NVT) ensemble. The NVE integration updates velocity and position of atoms based on the microcanonical ensemble [9]. (See the LAMMPS website for a detailed description for the NPT, NVT, and NVE commands). In short, the essential purpose of these commands is to allow the atoms to equilibrate (reach a comfortable position in the lattice) prior to

the non-equilibrium process of NEMD. The initial thermal equilibration was conducted

for 1.81 ns (determined appropriate by testing).

NEMD and Determination of Temperature Distribution

The steady state system is then disrupted by introducing a heat flux

$\left(74.074 \times 10^{-12} \text{ W/Å}^2\right)$. The application of heat is accomplished by increasing the

kinetic energy of the atoms in the hot zone and decreasing kinetic energy of the atoms in

the cold zone. This change in kinetic energy (a change in atom velocity) is equivalent to

adding thermal energy and removing thermal energy to the system. This process is

conducted in the NVE regime using the fix heat LAMMPS function.

The process is allowed to run until a new thermal equilibrium is reached, allowing

for the measurement of the thermal conductivity of the system. The baseline simulation

(discussed later) shows that for the particular system size described above, 13.2 ns were

sufficient for steady state after introducing the heat flux. During the final portion of

equilibration, the simulation values for temperature are recorded. These temperatures are

reported using the compute chunk/atom and the fix ave/chunk commands.

The compute chunk/atom command divides the test zone into chunks of equal

thickness in the z-dimension. The fix ave/chunk command evaluates the average (desired

property, in this case temperature) of all the atoms in each chunk. These values are saved

to a file along with the corresponding location (z-dimension) of the centroid of the chunk

in reference to the model axes.

The temperature values were reported and saved every 20 time steps. The average

temperature distribution was calculated from the results of the fix ave/chunk output by

finding the average value reported for each chunk.

<u>Determination of Thermal Conductivity</u>

Thermal conductivity of the steady state system can be found using the average temperature gradient (dT/dZ) and the known heat flux $\left(q = 74.074 \times 10^{-12} \text{ W/Å}^2\right)$. This is done by application of Fourier's Law.

$$q = -kA\frac{dT}{dZ} \qquad (3)$$

<u>Model Limitations</u>

The behaviors of atoms depend on a number of characteristics: atom spin, rotation, vibration and electronic modes. The simulations in this study include vibrational (solid structure, i.e., bonded atoms) and spin and rotational (gas, i.e., helium bubble simulation) energy modes. The electronic contributions to energy are not included in this particular LAMMPS MD simulation. The atoms are only modeled as point-masses. This influences the thermal conductivity values determined by the simulations. Thermal conductivity depends on the electron and phonon (lattice vibrations) contributions to thermal conductivity. For most ceramics and non-metals, the electronic contribution can be ignored. ZrC is an exception where the electron contribution is not negligible. The Wiedemann-Franz-Lorenz equation (Equation 4) gives the electron contribution of thermal conductivity. Equation 5 shows that total thermal conductivity, k_t, is equal to the summation of lattice thermal conductivity, k_{lat}, and electronic conductivity, k_{el}. Equation 4 can be used in conjunction with the k_t values reported in literature to determine k_{lat}. These k_{lat} values can then appropriately be compared with the results of this project. In Equation 4, σ is the electrical conductivity ($\Omega^{-1}\text{m}^{-1}$) at absolute temperature T (K) and L is the Lorenz number $2.44 \times 10^{-8} \text{ W}\Omega/\text{K}^2$. [6] [7].

$$k_{el} = L\sigma T \tag{4}$$

$$k_t = k_{el} + k_{lat} \tag{5}$$

The total thermal conductivity, k_t, reported from a literature survey by Harrison et al. is shown to range from 19-31 W/mK for 300 K and 25-39 W/mK for 1273 K [6]. the electron contribution to total thermal conductivity was found from the given electrical conductivity values also found in the work by Harrison et al. Table 3 summarizes the values by providing the range for k_{lat} found using equation 5. It was assumed that the maximum value for k_{lat} is found by subtracting the minimum k_{el} from the maximum value of k_t. (the opposite was done for the minimum value of k_{lat}).

Table 3: Reported values of k_t with associated lattice and electronic contributions and electrical conductivity

Temperature (K)	k_t (W/mK)	$\sigma \times 10^{-4}$ (Ω^{-1}m^{-1})	k_{el} (W/mK)	k_{lat} (W/mK)
300	19-31	119-158	9-12	8-22
1273	25-39	60-74	19-23	2-21

Sourced [6]:

BASELINE SIMULATION

The purpose of baseline simulation was threefold: first, to demonstrate the appropriateness of the ZrC interatomic potential selected for the project; second, to provide a comparison for all subsequent simulations; and third, to determine the time required to reach steady state. The simulation was determined to be stable after a run of 15ns that resulted in a steady temperature profile. The results can be seen in Figure 2. The dT/dZ term found in Equation 3 was determined by applying a linear curve fit to the linear region of the temperature profile given in Figure 2. (The R^2 value for this and all subsequent linear fits are above 0.9.)
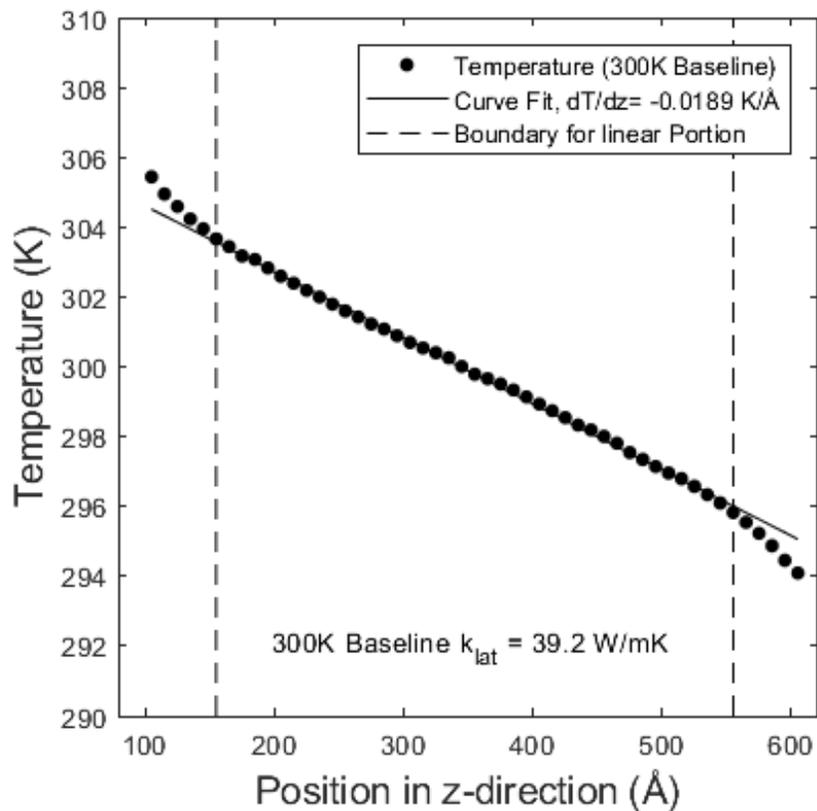

Figure 4: Temperature profile for the baseline case at 300K. Also included is the lattice thermal conductivity as calculated from the curve fit to the linear region as defined.

The boundary for the linear portion was selected to be 155-555 Å to avoid the non-linear regions near the boundaries of the hot and cold zones of the model. The effective baseline lattice thermal conductivity value is also shown in Figure 4.

The comparison of the baseline lattice thermal conductivity to the values reported in Table 3 show the baseline as over predicting the thermal conductivity of ZrC by as little as 17.2 W/mK to as much as 31.2 W/mK. The disparity, however, is justified as the MD simulation has a perfect crystal lattice while actual experiments are not guaranteed the same level of perfection due to grain boundaries, point defects, etc. The imperfections result in decreased thermal conductivity. By introducing pores in the next section, the disparity becomes less significant. This provides enough support that the baseline model and, by extension, the chosen interatomic potential are appropriate for the remaining simulations.

POROSITY SIMULATION

The effects of porosity on the lattice thermal conductivity of ZrC are investigated in this section. Porosity is adjusted by introducing spherical pores, or bubbles, to the crystal lattice. For this project, the pores are the all the same size (10 LC in Diameter or 46.98 Å). Four cases were investigated: one each for one, two, four, and six pores. The pores were placed within the center of the ZrC lattice and equally distributed in the z-direction along the same axis within the test zone of the model (see Figure 5).

Figure 5: A representation of the model simulation with the locations of empty bubbles for the 4 bubble case.

The porosity of each simulation was determined using Equation 4, where the porosity is given as the ratio of the volume of pores to the total volume measured [16].

$$\phi = V_p/V \qquad (4)$$

The porosity for each case in the porosity simulation is included in Table 4. The value for porosity is typically reported between zero and one. However, the values in Table 4 are written as percentages. The percent values reported in the table represent only the section of the test zone that is used for thermal conductivity measurements (155-555 Å). It should be noted that for the four and six pore cases, the 155-555 Å range partially cuts off the end pores, but the porosity values were calculated and adjusted accordingly.

Table 4: Simulation pore number and associated porosity

Number of Pores	Porosity (%)
0	0
1	3.1
2	6.3
4	10.8
6	18.1

Note: porosity found for volume represented by test zone measured from z = 155-555Å

The introduction of pores demands a more rigorous approach for determining the effective thermal conductivity of the lattice. This approach requires finding the thermal resistance for each section created by the pores (see Figure 6). Thermal resistance is defined as the overall resistance of a section to heat conduction. The equation for thermal resistance is given below, where L is the length, k is thermal conductivity, and A is the cross-sectional area of the particular section [16]

$$R = L/kA \tag{4}$$

The lattice thermal conductivity of each section is found in the same way as in the baseline study.

Thermal resistance provides a means for scaling the relative k_{lat} contributions of each section by the individual lengths of these sections. A summation of the thermal resistance of each section provides the total thermal resistance of the simulated lattice (for the total length being considered 155-555Å). Finally, the effective k_{lat} can be determined using Equation 4.
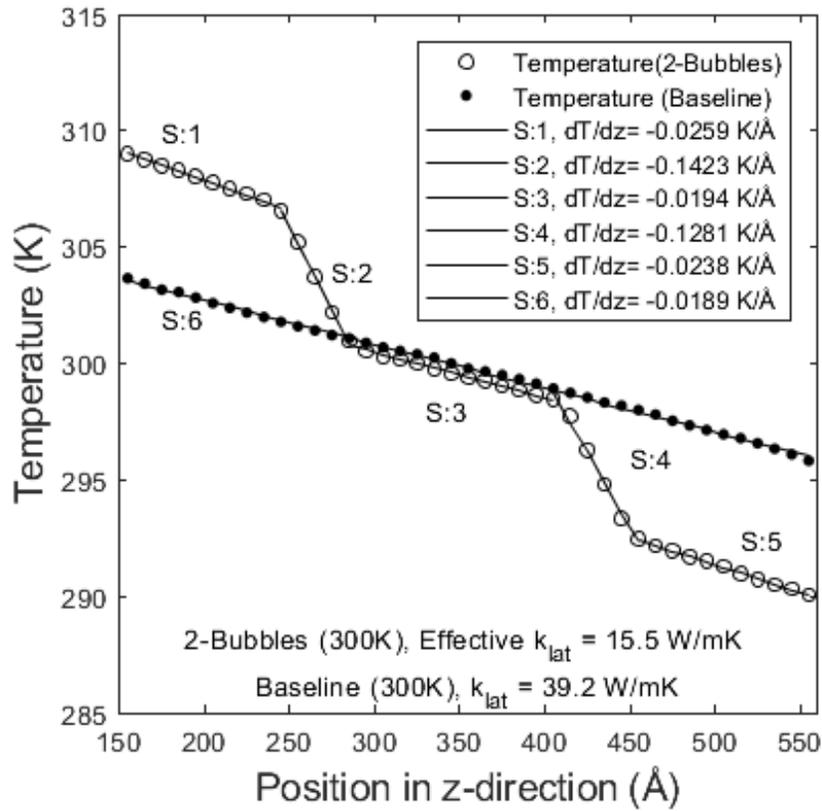
Figure 6: Plot of the temperature profile of the lattice for the 2-Bubble simulation (porosity = 6.3%) The location of the pores clearly indicated by the S:2 and S:3 regions.

Figure 6 shows the general method of analysis for all subsequent simulations with porosity greater than zero. Special care was taken to ensure the best linear fit for each section. It should be noted that the relative slopes for each section representing pores are nearly equivalent. The same can be stated for the sections representing the main undamaged ZrC structure. The collection of effective k_{lat} values found by this porosity simulation are reported in Figure 7. The reported values have been normalized by the baseline simulation k_t and plotted against the percent porosity of the middle 155-555 Å of the test zone.
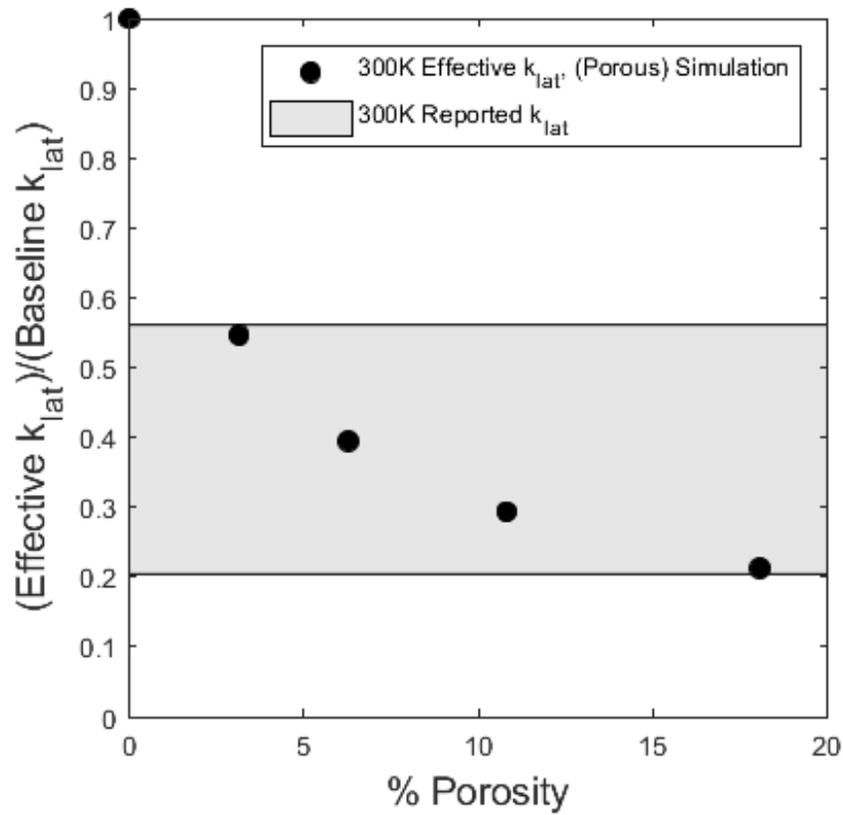
Figure 7: A Plot of normalized effective k_{lat} for the 300K porosity simulations.

The corresponding thermal conductivity to those plotted in Figure 7 are shown in Table 5 below. Just the addition of 1 pore (3.1% porosity) results in a 45% decrease in k_{lat}. However, the introduction of one pore results in a k_{lat} within the range of reported values of k_{lat}.

Table 5: Porosity simulation results (300K)

% Porosity	Effective k_{lat} (W/mK)
0	39.2
3.1	21.4
6.3	15.5
10.8	11.5
18.1	8.3

Reported values for k_{lat} range from 19-31 W/mK as mentioned earlier.

FISSION GAS SIMULATION

The addition of fission gas (helium), as discussed in the introduction, has value in modeling the behavior of ZrC due to radiation exposure. Each pore in the simulation is filled with helium to approximate density of 0.8×10^{28} atoms/m^3. The results show a slight increase in the thermal conductivity over the empty pores.
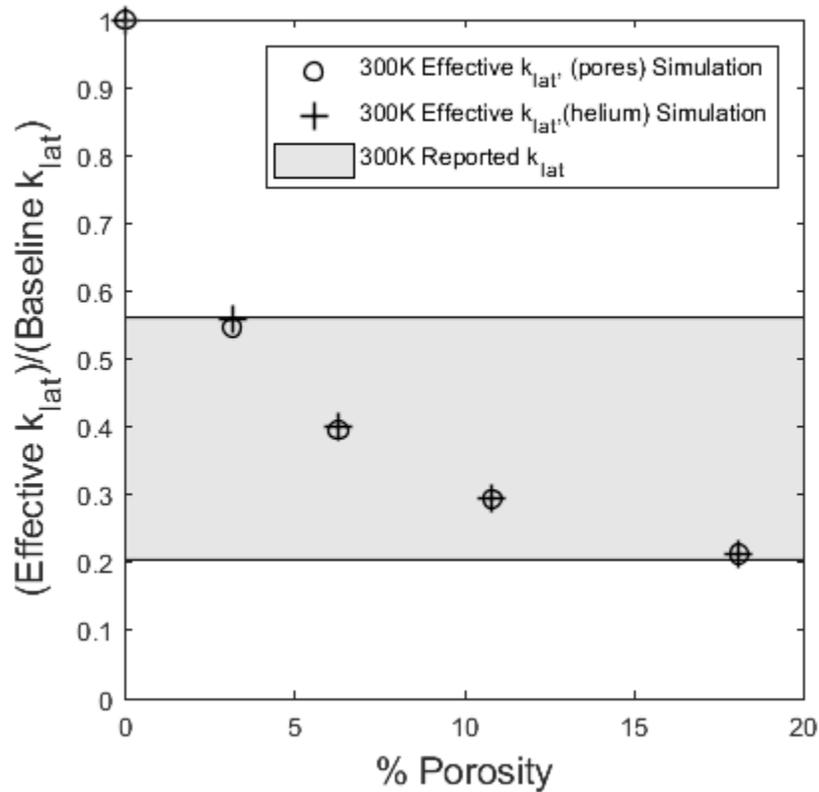

Figure 8: The compiled results of the fission gas simulation (300K). The (300K) porosity simulation results are also included for reference.

The values of k_{lat} shown in Figure 7 can be found in Table 6 below. The effect of helium in this particular model has very little effect on the thermal conductivity of the system. The percent increase in k_{lat} is also shown in Table 6.

Table 6: Fission gas simulation results (300K)

% Porosity	Porosity Simulation Effective k_{lat} (W/mK)	Fission Gas Simulation Effective k_{lat} (W/mK)	% Increase
0	39.2	39.2	NA*
3.1	21.4	21.9	2.3
6.3	15.5	15.7	1.3
10.8	11.5	11.6	0.9
18.1	8.3	8.4	1.2

*Not applicable to baseline values

HIGH TEMPERATURE SIMULATION

The final simulations were raised to the temperature of 1273K. This temperature value was selected as the appropriate value based on the limitations of TRISO fuels. The highest operational temperature for the TRISO fuel is limited to 1250K (1523°C), and VHTRs are anticipated to have outlet temperatures of 1273K (1000°C) [18]. This simulation repeats all the cases for filled and empty pores at the elevated temperature. The compiled results are shown in Figure 9.
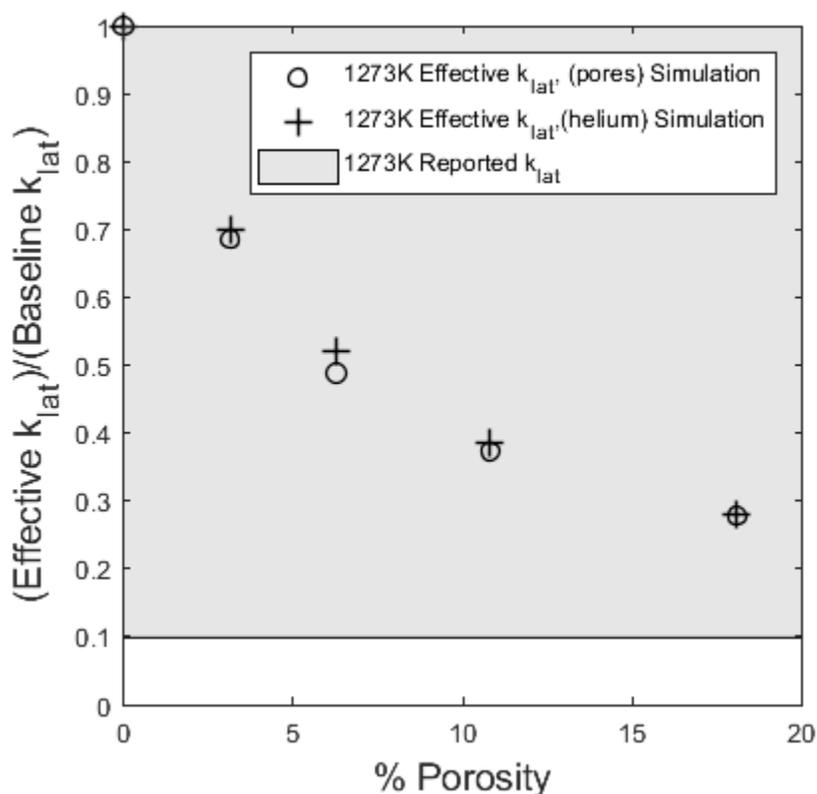

Figure 9: The compiled results of the high temperature simulations compared to the values found in the literature.

Again, there is very little impact from the addition of helium. Table 7 shows the percent increase for each case. The values of percent increase are higher than those of the 300K simulations and are likely due to the increased kinetic energy of the atoms of the

system. Particularly, helium atoms are likely moving much faster and contributing more to the transfer of energy in the system than at the lower temperature simulations. Also, the overall effective k_{lat} values found for the high temperature simulations are much lower than those found for the low temperature simulations. This follows the trend that phonon contribution to k_{lat} tends to decrease with increasing temperature, and is a result of the anharmonic lattice vibrations that arise and with elevated temperatures causing phonon scattering [6].

Table 7: High temperature simulation Results

% Porosity	Porosity Simulation Effective k_{lat} (W/mK)	Fission Gas Simulation Effective k_{lat} (W/mK)	% Increase
0	20.3	20.3	NA*
3.1	13.9	14.2	2.2
6.3	9.9	10.6	7.1
10.8	7.6	7.8	2.6
18.1	5.6	5.7	1.8

*Not applicable to baseline values

SUMMARY AND CONCLUSION

A NEMD model was developed for finding the k_{lat} of ZrC. The model demonstrates the effects of porosity and, to a minor degree, the effects of helium-filled pores on the thermal conductivity of a ZrC lattice. The compiled results of the project can be seen in Figure 10.
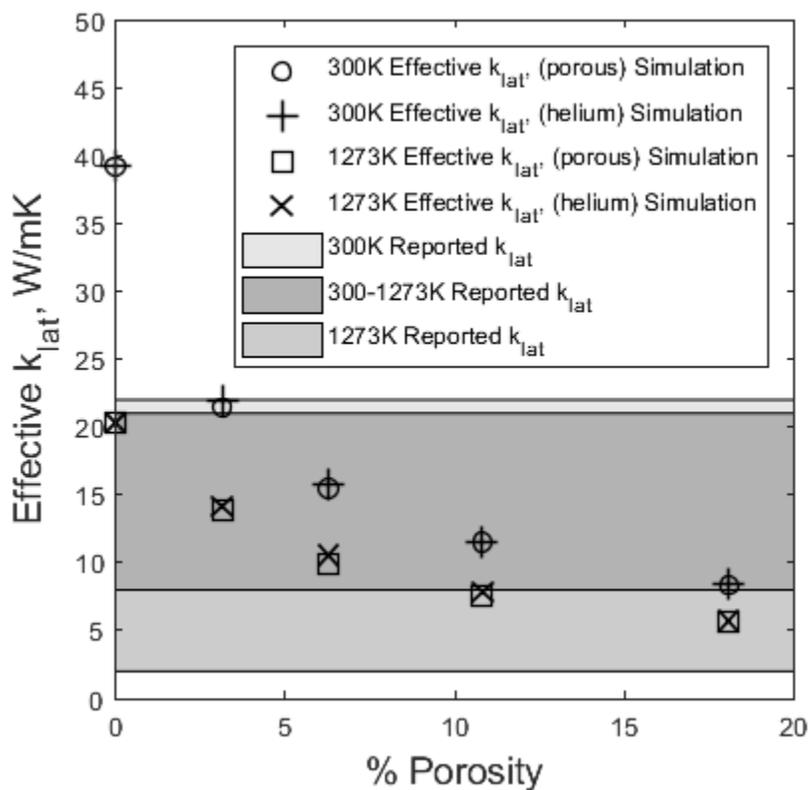

Figure 10: Combined high and low temperature simulation results, including the range of k_{lat} values reported in the literature for the respective temperature ranges.

The figure shows that with increased porosity there is a decrease in effective k_{lat}. The initial decrease in effective k_{lat} from the baseline value is quite large (~45% for the low temperature simulations and ~32% for the high temperature simulations). All subsequent increases in porosity have less significant changes to the effective k_{lat}. This

behavior of decreasing thermal conductivity is attributed primarily to phonon scattering at the boundaries of the pores. Though the decrease from the baseline value is significant, all other values reported in the study fall within the range of k_{lat} reported in the literature.

The effects of phonon scattering are also evident in the baseline simulations. The high temperature case shows a lower baseline k_{lat}. This is due to the increase in phonon scattering from anharmonic lattice vibrations associated with elevated temperatures.

The addition of helium to the pores provide an increase in k_{lat}. The increase is rather small but can be attributed to the atoms available for transferring energy where otherwise existed empty pores. The high temperature simulations show the greatest improvement to effective k_{lat} with the addition of helium. The results show a 7% increase in the effective k_{lat} over the empty pores (for the 6.3% porosity case). However, this only accounts for approximately a 0.7 W/mK increase in k_{lat}.

The chosen geometry and helium density limit the results of the simulation; however the results of the work do provide sufficient information regarding the effects of helium filled pores on the k_{lat} of ZrC. The use of ZrC as a cladding material in nuclear fuel runs the risk of having significant drops in thermal conductivity over time. There is a slight increase in thermal conductivity from the presence of fission gas in the pores. Despite the increase, the overall drop in k_{lat} is dominated by the existence of the pores (or microstructural damage).

REFERENCES

[1] Forum, U.S. DOE Nuclear Energy Research Advisory Committee and the Generation IV International, "A Technology Roadmap for Generation IV Nuclear Energy Systems," 2002.

[2] D. Kim, M. J. Ko, J. Y. Park, M. S. Cho and W.-J. Kim, "Influence of free carbon on the characteristics of ZrC and deposition of near-stoichiometric ZrC in TRISO coated particle fuel," *Journal of Nuclear Materials,* vol. 451, pp. 97-103, 2014.

[3] W. E. Lee, M. Gilbert, S. T. Murphy and R. W. Grimes, "Opportunities for Advanced Ceramics and Composites in the Nuclear Sector," *Journal of the American Ceramic Society,* vol. 96, no. 7, pp. 2005-2030, 11 June 2013.

[4] T. Besmann, *Thermochemical Behaviour of Oxide Nuclear Fuel to High Burn-up: Effect of Lanthanides,* Columbus, OH, 2011.

[5] I. E. Porter, T. W. Knight, M. C. Dulude, E. Roberts and J. Hobbs, "Design and fabrication of an advanced TRISO fuel with ZrC coating," *Nuclear Engineering and Design,* vol. 259, pp. 180-186, June 2013.

[6] R. W. Harrison and W. E. Lee, "Processing and properties of ZrC, ZrN and ZrCN: a review," *Advances in Applied Ceramics,* vol. 115, no. 5, pp. 294-307, 2016.

[7] C. Jensen, M. Chirtoc, N. Horny, J. S. Antoniow, H. Pron and H. Ban, "Thermal conductivity profile determination in proton-irradiated ZrC by spacial and frequency scanning thermal wave methods," *Journal of Applied Physics,* vol. 114, no. 13, pp. 133509-133509-9, Oct 2013.

[8] C. -W. Lee, A. Chernatynskiy, P. Shukla, R. Stoller, S. Sinnott and S. Phillpot, "Effect of pores and He bubbles on the thermal transport properties of UO2 by molecular dynamics simulation," *Journal of Nuclear Materials,* vol. 456, pp. 253-259, 2015.

[9] "LAMMPS Molecular Dynamics Simulator," [Online]. Available: http://lammps.sandia.gov/. [Accessed April 2018].

[10] "Interatomic Potentials Repository Project," National Institute of Standards and Technology, 2018. [Online]. Available: https://www.ctcms.nist.gov/potentials/.

[11] A. I. Duff, M. Finnis, P. Maugis, B. J. Thijsse and M. H. Sluiter, "MEAMfit: A reference-free modified embedded atom method (RF-MEAM) energy and force-fitting code," *Computer Physics Communications,* vol. 196, pp. 439-445, 2015.

[12] T. S. Jakubov and D. E. Mainwaring, "Direct calculations of the dispersion interaction between fullerenes and their equation for the potential energy," *Adsorption,* vol. 14, no. 4-5, pp. 727-732, 2008.

[13] M. Balasubramanya, M. Roth, P. Tilton and B. Suchy, "Molecular dynamics simulations of noble gas release from endohedral fullerene clusters," 2006.

[14] L. Xie, P. Brault, A.-L. Thomann and L. Bedra, "Molecular dynamic simulation of binary ZrxCu100−x metallic glass thin film growth," *Applied Surface Science,* vol. 274, pp. 164-170, 2013.

[15] C. P. Kempter and R. J. Fries, "Crystallographic Data. 189. Zirconium Carbide," *Analytical Chemistry,* vol. 32, no. 4, pp. 570-570, 1960.

[16] E. J. Garboczi, D. P. Bentz and N. S. Martys, "Digital images and computer

Updated 20180503

Modeling," in *Experimental Methods in the Physical Sciences*, P. Wong, Ed., New York: Academic Press, 1999, pp. 1-41.

[17] F. P. Incropera, D. P. Dewitt, T. L. Bergman and A. S. Lavine, Fundamentals of Heat and Mass Transfer, 6th ed., John Wiley & Sons, Inc., 2007.

[18] I. A. E. Agency, "High Temperature Gas Cooled Reactor Fuels and Materials IAEA-TECDOC-1645," IAEA, Vienna, 2010.